

Fabrication of 200 nm period blazed transmission gratings on silicon-on-insulator wafers

Minseung Ahn,^{a)} Ralf K. Heilmann, and Mark L. Schattenburg
Massachusetts Institute of Technology, Cambridge, Massachusetts 02139

(Received 17 June 2008; accepted 14 July 2008; published 1 December 2008)

The authors report on the fabrication of 200 nm period blazed transmission gratings on silicon-on-insulator (SOI) wafers. These critical angle transmission (CAT) gratings require 3–5 μm tall freestanding grating bars with a very high aspect ratio (>100) and smooth sidewalls. In order to meet the challenging geometrical requirements, they modified and improved our previously reported process for the fabrication of a CAT grating prototype with 574 nm period. They have used potassium hydroxide (KOH) solutions to fabricate high aspect ratio gratings on $\langle 110 \rangle$ SOI wafers. The KOH etching process was improved to minimize the lateral undercut through precise grating alignment to $\langle 111 \rangle$ planes within $\pm 0.05^\circ$ and a room temperature etch process with 50 wt % KOH. In addition, an image-reversal technique with a high silicon content spin-on polymer was applied to increase process latitude with a high duty cycle nitride mask. A surfactant was also added to the KOH solution to promote hydrogen bubble release. With the improved process, they achieved a high etch anisotropy of above 300 on a $\langle 110 \rangle$ silicon wafer. They successfully fabricated 200 nm period CAT gratings with support mesh periods of 25 and 40 μm in a 9 mm² area of 4- μm -thick silicon membranes on $\langle 110 \rangle$ SOI wafers. © 2008 American Vacuum Society. [DOI: 10.1116/1.2968613]

I. INTRODUCTION

Diffraction gratings have been widely used for space instrumentation to analyze x rays radiated from various celestial objects.^{1–6} Combining the advantages of transmission and reflection gratings, we have developed a new high-efficiency transmission grating for the extreme ultraviolet to soft x-ray band, which requires freestanding grating bars with very high aspect ratios (>100) and smooth sidewalls.^{7,8} We have previously introduced the concept of this critical-angle-transmission (CAT) grating⁷ and fabricated 574 nm period CAT grating prototypes on 10- μm -thick SOI wafers.⁸ Diffraction tests of these gratings with low energy x rays (<0.5 keV) have shown high-efficiency blazing as predicted by theory.⁷ However, for higher energy x-ray applications, shorter period CAT gratings with a duty cycle (linewidth/period) less than 0.2 are desired.⁹ Therefore, we need to adapt the previous process to the fabrication of 200 nm period CAT gratings with 40 nm linewidth.

We have used KOH etching on $\langle 110 \rangle$ SOI wafers to achieve straight and high aspect ratio freestanding gratings. In order to achieve 4- μm -tall and 40-nm-wide grating bars by etching, etch anisotropy between $\langle 110 \rangle$ and $\langle 111 \rangle$ silicon crystal lattice planes should be at least 200, considering the silicon nitride mask linewidth (<100 nm) formed by interference lithography and reactive-ion etch (RIE), as well as undercut during KOH etching. The etch rate anisotropy in KOH solutions dramatically varies depending on pattern alignment to the $\langle 111 \rangle$ direction, the KOH concentration, and etching temperature.^{10,11} We also found that there was a rapid initial undercut, which impaired the etch anisotropy. We investigated these factors to optimize the KOH etch process for

etching the 200 nm grating pattern. In order to increase the etch process latitude through increased linewidth, we applied an image-reversal technique with a high silicon content spin-on polymer, Silspin (Molecular Imprints, TX). A surfactant, sodium dihexyl sulfosuccinate (SDSS), was added to KOH solutions to promote hydrogen bubble release.

In the following, we will describe the process improvements in detail and demonstrate a CAT grating with a 200 nm period on wafers with a 25 μm pitch support mesh on a 4- μm -thick SOI layer.

II. FABRICATION

Our substrates were 100 mm diameter $\langle 110 \rangle$ SOI wafers (Ultrasil, Hayward, CA) with a 4 μm device layer, 2 μm buried oxide, and 500 μm handle layer. The wafer has two flats in the $\langle 111 \rangle$ directions with $\pm 0.2^\circ$ tolerance. The fabrication process consists of four substeps, comprising front side patterning, backside patterning and etch with tetramethylammonium hydroxide (TMAH), front side etch with KOH, and release with critical point drying. The original fabrication process, developed for a prototype with a larger period, was described in detail in Ref. 8. We modified this fabrication process to attain 200 nm period CAT gratings. Since the KOH etch anisotropy is affected by pattern alignment to the $\langle 111 \rangle$ crystal direction, ahead of the grating patterning process a preetch technique¹² was utilized with a fan-shape pattern with 0.05° angular spoke spaced over the range of $\pm 3^\circ$ so as to find the actual $\langle 111 \rangle$ direction rather than relying on the wafer flat. Figures 1(a) and 1(b) show the fan-shape pattern in the photoresist on top of a silicon nitride (SiN) layer and a single spoke after 30 min KOH (20 wt %) etch at 80 °C, respectively. Measuring the undercut using scanning electron microscopy (SEM), we can find the $\langle 111 \rangle$

^{a)}Electronic mail: msahn@mit.edu

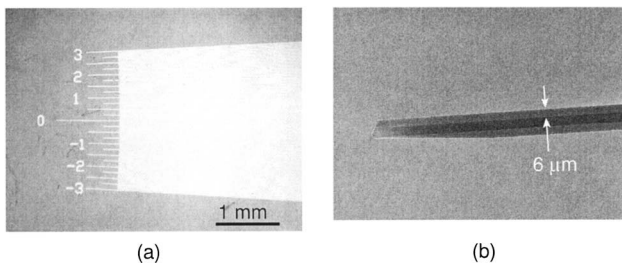


FIG. 1. Micrograph of the fan-shape mask pattern (a) before KOH etching and (b) a single spoke after KOH etching. 40-nm-thick nitride is partially transparent at 5 keV SEM voltage and the undercut is measurable in the top view.

direction, as shown in Fig. 2, which will be used as an alignment key in the following interference lithography step for patterning the 200 nm period grating.

The 200 nm period grating pattern with a duty cycle of less than 20% was reversed using the Silspín and RIE processes to form a wider nitride mask, as shown in Fig. 3. By using the spin-on polymer, we obtain better pattern uniformity within the wafer compared to metal evaporation with a point source and a lift-off process. In the image-reversal process, the photoresist pattern is first transferred into the anti-reflection coating (ARC) [Fig. 3(a)]. The remaining photoresist can be left on because it will be dissolved by the Silspín or optionally removed by *n*-methyl-2-pyrrolidone. Silspín is conformally spin coated on the ARC pattern [Fig. 3(b)]. Using CF_4 and O_2 RIE consecutively, the pattern is transferred into nitride and silicon [Figs. 3(c)–3(e)]. The remaining Silspín can be removed by piranha cleaning (sulfuric acid+hydrogen peroxide). The duty cycle of the image-reversed pattern is about 70%. Figure 4 shows the final etch mask with a support mesh and 200 nm period grating in a nitride layer.

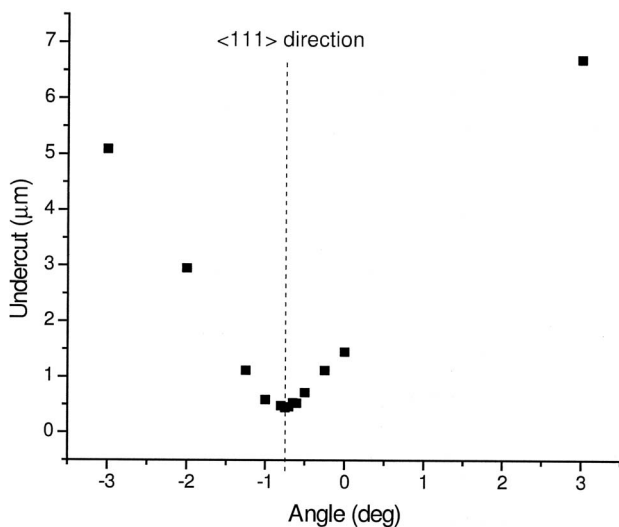


FIG. 2. Example of determination of the actual $\langle 111 \rangle$ direction of a $\langle 110 \rangle$ wafer using the preetched fan-shape pattern. The minimum undercut direction can be assumed to be parallel to a $\{111\}$ plane. In this example, the actual $\{111\}$ plane is -0.75° off from the fan's 0° direction.

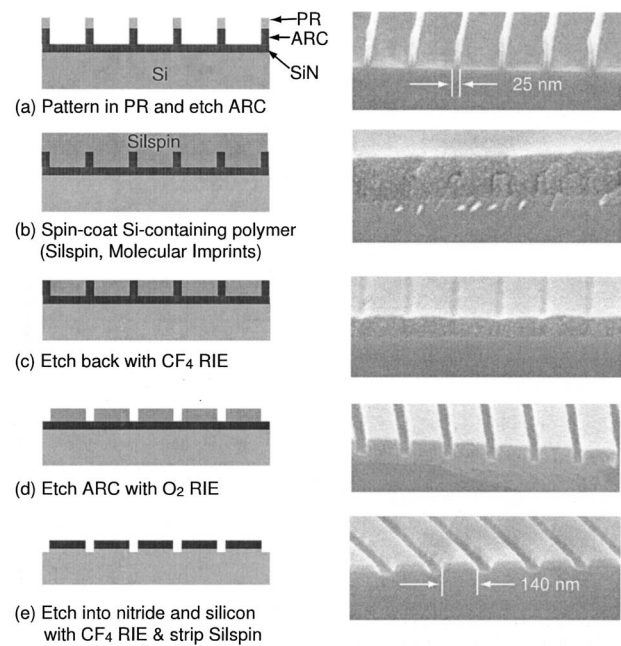


FIG. 3. Schematic and SEM images of an image-reversal technique using a Si-containing polymer. The duty cycle of the 200 nm period grating pattern is reversed from 12.5% in photoresist and ARC to 70% in silicon nitride.

After patterning and etching the backside of the SOI wafer,⁸ we performed KOH etching with a surfactant-added 50 wt % KOH solution at room temperature ($\sim 21^\circ\text{C}$) for 4 h to etch through the $4\text{-}\mu\text{m}$ -thick device layer. The surfactant, SDSS (MA-80I, Cytec Inc., West Peterson, NJ), was applied to improve etch uniformity by promoting hydrogen bubble release during KOH etching.¹³ Figure 5 shows the

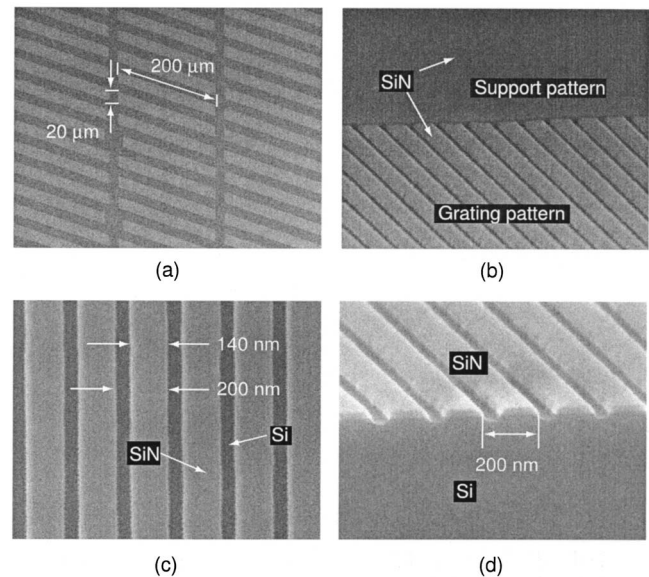


FIG. 4. SEM images of the front side nitride etch mask with support mesh pattern and 200 nm period grating. (a) Support mesh pattern with an array of $20 \times 20 \mu\text{m}^2$ grating areas, (b) blow-up of the interface between the support pattern and grating, (c) top view of the 200 nm period grating, and (d) cross section of (c).

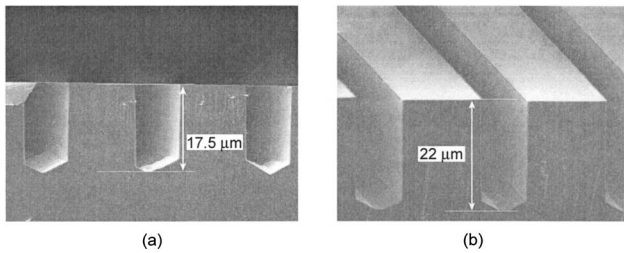


FIG. 5. SEM images of fan-shape pattern etched for 16 h at room temperature (a) in 50 wt % KOH without the surfactant and (b) in 50 wt % KOH +0.02 wt % SDSS.

effect of the surfactant. The etch bottom is bumpy and irregular without the surfactant [Fig. 5(a)]. On the other hand, 0.02 wt % of SDSS in 50 wt % KOH solution made the etch front much smoother and more uniform [Fig. 5(b)].

The process ends with a removal of the nitride mask and buried oxide using hydrofluoric acid (48% HF), followed by critical point drying as described in Ref. 8.

III. RESULTS AND DISCUSSION

In order to find an optimum KOH etching condition, we investigated etch anisotropy dependency on KOH concentration, temperature, and pattern alignment by etching the fan-shape patterns under four different conditions, as shown in Fig. 6. The anisotropy was determined by the ratio of etch depth to the undercut amount. We observed that higher concentrations and lower temperatures resulted in higher etch anisotropy. The pattern alignment was also one of the most important factors in obtaining high etch anisotropy. However, even the best anisotropy values in Fig. 6 were less than literature values^{10,14} and below our process requirement (>200). Therefore, we conducted a timed etching experiment with a 200 nm period grating to investigate the low etch anisotropy problem. The grating used was well aligned by the preetch technique and etched in the surfactant-added

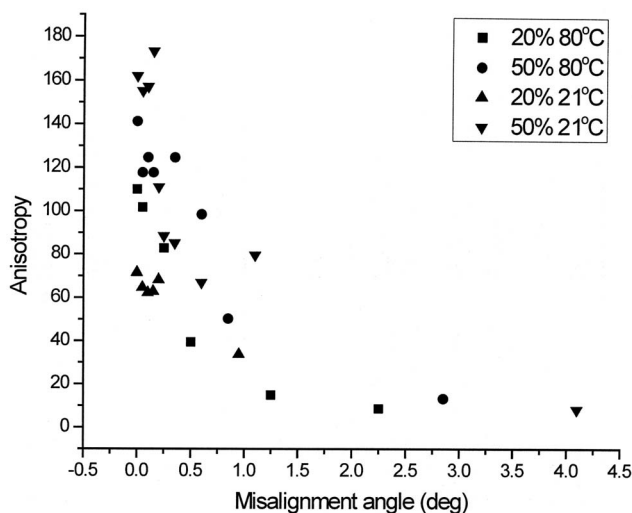


FIG. 6. Etch anisotropy between $\langle 110 \rangle$ and $\langle 111 \rangle$ planes at different etching conditions and pattern misalignment with respect to the $\langle 111 \rangle$ plane.

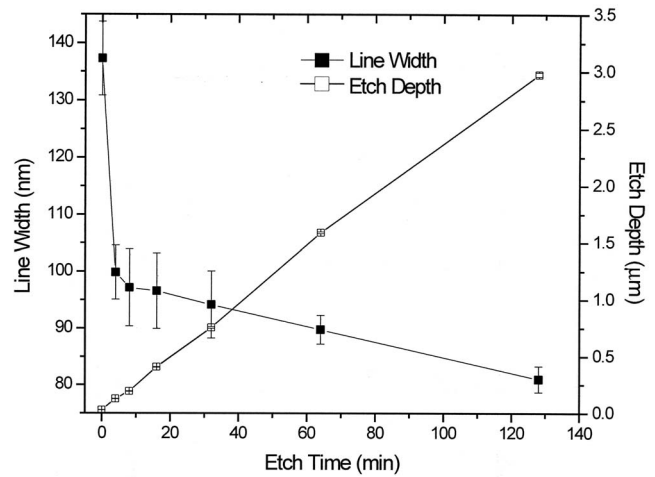


FIG. 7. Etched grating linewidth and depth with increasing etching time. The etch depth (open squares) increases linearly, so the vertical etch rate, $R_{\langle 110 \rangle}$, stays constant at about $1.4 \mu\text{m}/\text{h}$. However, the linewidth (full squares) drops very rapidly in the first few minutes and slows to a constant rate, which should correspond to the actual $\langle 111 \rangle$ etch rate ($R_{\langle 111 \rangle}$). The initial undercut rate and the actual $R_{\langle 111 \rangle}$ are about $4.6 \text{ nm}/\text{min}$ and $4.3 \text{ nm}/\text{h}$, respectively.

50 wt % KOH at room temperature. At each time shown in the plot, we measured the silicon linewidth from the top after removing the nitride, and the etch depth after cleaving. Figure 7 shows that there is a very rapid initial undercut, which might be caused by mask roughness. After about 10 min of etch, the lateral etch rate approaches a roughly constant rate of $4.3 \text{ nm}/\text{h}$, which is assumed to be the actual $\langle 111 \rangle$ etch rate. The $\langle 110 \rangle$ etch rate (open squares) in Fig. 7 was relatively constant at about $1.4 \mu\text{m}/\text{h}$. An etch anisotropy of about 325 is obtained from the ratio of these etch rates. It is clear that the anisotropy values in Fig. 6 are inaccurate because the lateral etch rate had been determined by including the initial rapid undercut from the initial mask linewidth roughness.

We successfully fabricated a 200 nm period CAT grating in a $4\text{-}\mu\text{m}$ -thick device layer of a SOI wafer. Figure 8 shows the top, bottom, and cross-section views of the freestanding CAT grating. The open gap between the support lines was $20 \mu\text{m}$ at the top and $5 \mu\text{m}$ at the bottom, which agrees well with the silicon crystal angle for inclined $\{111\}$ planes. The linewidths of a single grating bar are 35 nm at the top and 45 nm at the bottom. The aspect ratio of the grating bar is about 100 with a sidewall slope angle of 0.07° , which implies a very high etch anisotropy. To the best of our knowledge, the sidewall slope in this scale is the steepest reported angle that has been achieved by any etching technique.

IV. CONCLUSION AND FUTURE WORK

We have significantly improved the previous fabrication process and demonstrated a 200 nm period CAT grating on the $4\text{-}\mu\text{m}$ -thick device layer of a $\langle 110 \rangle$ SOI wafer. A high etch anisotropy was achieved using a high concentration KOH solution with surfactant at room temperature to enable vertically etching a well aligned grating pattern. An image-

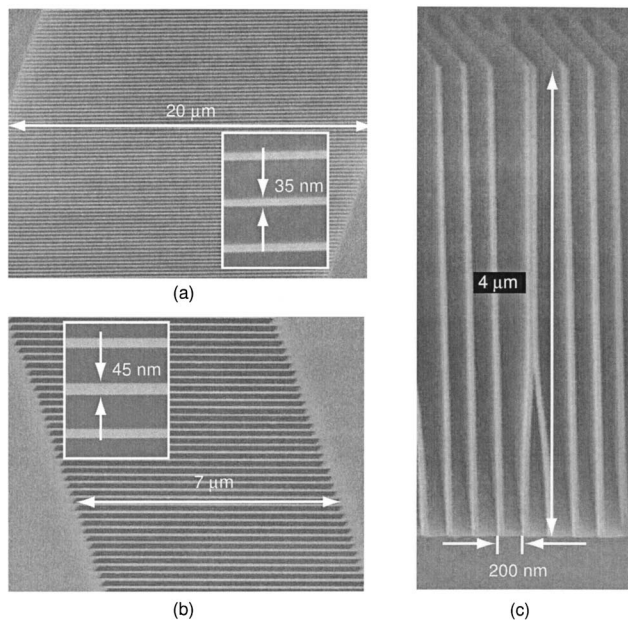


FIG. 8. SEM images of a 200 nm period blazed freestanding transmission grating in a 4- μm -thick (110) silicon-on-insulator substrate. (a) Top view of the fine grating between a 20 μm open gap. The linewidth at the top is 35 nm. (b) Bottom view of the grating. The open gap has shrunk to $\sim 7 \mu\text{m}$ due to the slanted {111} planes. The linewidth is 45 nm, which is consistent with an average sidewall slope of $\sim 0.07^\circ$. (c) Cross section of the grating. The stiction is due to cleaving.

reversal technique with a spin-on polymer increased process latitude. This CAT grating with 9 mm² area will be tested with soft x rays to demonstrate the blazing effect. Furthermore, we believe that we have enough process latitude to successfully apply this fabrication technique to thicker device layers for even higher aspect-ratio grating bars.

ACKNOWLEDGMENTS

The authors gratefully acknowledge the assistance of Robert Fleming and Chih-Hao Chang of the MIT Space Nanotechnology Laboratory and James Daley of the MIT NanoStructures Laboratory. Staff and facility support from the Space Nanotechnology Laboratory, NanoStructures Laboratory, and Microsystems Technology Laboratories at MIT are also appreciated. This work is supported by NASA Grant No. NNX07AG98G, Kavli Instrumentation and Technology Development Fund, and a Samsung Scholarship.

- ¹M. L. Schattenburg, C. R. Canizares, D. Dewey, K. A. Flanagan, M. A. Hamnett, A. M. Levine, K. S. K. Lum, R. Manikkalingam, T. H. Markert, and H. I. Smith, *Opt. Eng. (Bellingham)* **30**, 1590 (1991).
- ²M. L. Schattenburg, *J. Vac. Sci. Technol. B* **19**, 2319 (2001).
- ³R. Giacconi, G. Branduardi, U. Briel, A. Epstein, D. Fabricant, E. Feigelson, W. Forman, P. Gorenstein, J. Grindlay, H. Gursky *et al.*, *Astrophys. J.* **230**, 540 (1979).
- ⁴M. C. Weisskopf, *Proc. SPIE* **5488**, 25 (2004).
- ⁵C. R. Canizares, J. E. Davis, D. Dewey, K. A. Flanagan, E. B. Galton, D. P. Huenemoerder, K. Ishibashi, T. H. Markert, H. L. Marshall, M. McGuiirk *et al.*, *Publ. Astron. Soc. Pac.* **117**, 1144 (2005).
- ⁶J. W. den Herder, A. C. Brinkman, S. M. Kahn, G. Branduardi-Raymont, K. Thomsen, H. Aarts, M. Audard, J. V. Bixler, A. J. den Boggende, J. Cottam *et al.*, *Astron. Astrophys.* **365**, L7 (2001).
- ⁷R. K. Heilmann, M. Ahn, E. M. Gullikson, and M. L. Schattenburg, *Opt. Express* **16**, 8658 (2008).
- ⁸M. Ahn, R. K. Heilmann, and M. L. Schattenburg, *J. Vac. Sci. Technol. B* **25**, 2593 (2007).
- ⁹K. Flanagan, M. Ahn, J. Davis, R. Heilmann, D. Huenemoerder, A. Levine, H. Marshall, G. Prigozhin, A. Rasmussen, G. Ricker *et al.*, *Proc. SPIE* **6688**, 66880Y (2007).
- ¹⁰D. L. Kendall, *Annu. Rev. Mater. Sci.* **9**, 373 (1979).
- ¹¹P. Krause and E. Obermeier, *J. Micromech. Microeng.* **5**, 112 (1995).
- ¹²H. Seidel, L. Csepregi, A. Heuberger, and H. Baumgartel, *J. Electrochem. Soc.* **137**, 3626 (1990).
- ¹³C.-R. Yang, P.-Y. Chen, Y.-C. Chiou, and R.-T. Lee, *Sens. Actuators, A* **119**, 263 (2005).
- ¹⁴M. J. Madou, *Fundamentals of Microfabrication: The Science of Miniaturization*, 2nd ed. (CRC, Boca Raton, FL, 2002).